Cyclotron resonance in rare-earth monopnictides

Makoto Yoshida* and Keiichi Koyama
High Field Laboratory for Superconducting Materials, Institute for Materials Research, Tohoku University, Sendai 980-8577, Japan

Akira Ochiai
Center for Low Temperature Science, Tohoku University, Sendai 980-8578, Japan

Mitsuhiro Motokawa
Institute for Materials Research, Tohoku University, Sendai 980-8577, Japan
(Received 8 January 2004; revised manuscript received 5 October 2004; published 2 February 2005)

Recently, we have developed equipment which can be used for both cyclotron resonance (CR) and electron spin resonance (ESR) measurements for studying *f*-electron systems. Using this equipment and preparing high-quality single crystals with a residual resistivity ratio of about 500, we have successfully observed CR signals in rare-earth monopnictides *RX* (R=La, Ce, Pr, Gd, X=Sb, Bi). The purpose of this paper is to describe the development of our measurement system in detail and to reexamine our recent results of CR measurements on the single crystals of *RX*. And then, we discuss the origin of mass enhancement in this system by comparing the case of a strongly correlated *f*-electron system CeSb with the case of a nonmagnetic simple semimetal LaSb. The CR measurements have been performed in the temperature range from 1.4 K to 40 K and in the frequency range from 50 to 190 GHz. We have observed CR signals in LaSb, LaBi, CeSb, PrSb, and GdSb. The cyclotron effective masses m^*_{CR} determined by the CR measurements are compared with the masses m^*_{QO} estimated by measurements of quantum oscillations and the masses m^*_{BC} deduced from band structure calculations. The determined m^*_{CR} of LaSb, LaBi, and GdSb is in the range of $(0.17-0.65)m_0$. These values are reasonably consistent with the values of m^*_{QO} and m^*_{BC}. This fact shows that both m^*_{CR} and m^*_{QO} mainly depend on the band structure if the interaction between conduction electrons and *f* electrons is negligible. On the other hand, in the case of a strongly correlated *f*-electron system CeSb, m^*_{CR} is in the range of $(0.26-1.5)m_0$. These values are much larger than those of m^*_{BC}. This finding shows that m^*_{CR}, as well as m^*_{QO}, is considerably enhanced in CeSb. Our results indicate that the interband interaction is important for the mass enhancement of m^*_{CR} in CeSb.

DOI: 10.1103/PhysRevB.71.075102 PACS number(s): 71.18.+y, 71.27.+a, 76.40.+b

I. INTRODUCTION

Measurements of quantum oscillations (QO) such as the de Haas–van Alphen (dHvA) and Shubnikov–de Haas (SdH) effects are powerful methods to investigate the Fermi surface of metals. These experiments can determine the extremal cross-sectional area, the cyclotron effective mass, the mean free path, and so on. On the other hand, cyclotron resonance (CR) is considered to be the best method to determine the cyclotron effective mass of substances. In addition, CR measurements are supposed to give us other information about the carriers at the Fermi surface.[1–13] In particular, the effective mass (m^*_{CR}) determined by CR measurements is considered to be different from the mass (m^*_{QO}) estimated from dHvA or SdH effect measurements. According to the Kohn's theorem[12] for electron motion in a Galilean-invariant electron gas, m^*_{CR} is independent of the electron-electron interaction, whereas m^*_{QO} is additionally influenced by the interaction. In this case, m^*_{CR} is supposed to be smaller than m^*_{QO}. Therefore, it is important to investigate not only m^*_{QO} but also m^*_{CR} in strongly correlated electron systems. Recently, some research groups have performed CR measurements in organic conductors and Sr_2RuO_4, and compare m^*_{CR} with m^*_{QO}.[1–3,7,9,10] However, there have been only a few reports of CR experiments for rare-earth or uranium compounds, because CR measurements of metallic compounds are difficult and sometimes very complicated. In this work, therefore, we have systematically studied the CR of rare-earth monopnictides to obtain information on the Fermi surface, effective mass, electron-electron interaction, and so on.

Rare-earth monopnictides *RX* (R=rare earth, X=N, P, As, Sb, and Bi) with NaCl-type crystal structure are typical systems with low carrier density. Several compounds of *RX* show unusual physical properties such as dense Kondo behavior, heavy fermion state, complicated magnetic states, and so on.[14–17] As is well known, the effect of electron-electron interactions plays an important role in the systems. There are a number of reports of dHvA or SdH effect measurements for *RX*, and band structure calculations for them have also been performed.[18–34] These experimental and theoretical studies show that *RX* compounds have very simple Fermi surfaces. Except for Ce and Yb monopnictides, the Fermi surface topology is same as that of a nonmagnetic reference compound LaSb, which is studied by the dHvA measurements and the band structure calculation in details.[18–20] The Fermi surface of LaSb consists of three branches α, β, and γ. The α branch is the electron Fermi surface with an ellipsoidal shape at the X point. The β branch is the hole Fermi surface which is almost spherical and centered at the Γ point. The γ branch is also the hole surface at the Γ point and slightly elongated along the $\langle 100 \rangle$ direction.

TABLE I. The effective masses m^*_{QO} determined by the dHvA effect measurements for CeSb taken from Refs. 36 and 26 and the masses m^*_{BC} calculated for CeSb (Ref. 29). m_0 is the free electron mass.

CeSb Branch	$m^*_{QO}(m_0)$ $B\|[001]$	$m^*_{BC}(m_0)$ $B\|[001]$
AFF2 phase		
	0.2[a]	-
	0.3[a]	-
	0.3[a]	-
AFF1 phase		
α'	0.13[b]	0.06[c]
γ'_{low}	-	-
γ'_{high}	0.69[b]	0.45[c]
β'	0.71(high)[b]	0.29[c]
	0.65(low)[b]	0.27[c]
β'_3	1.2[b]	0.52[c]
β'_4	1.4[b]	0.51[c]
δ	1.1[b]	0.24[c]
F phase		
α	0.23±0.02[b]	0.14[c]
γ(high)	0.8±0.1[b]	0.47[c]
γ(low)	0.9±0.1[b]	0.46[c]
β_1	0.5±0.05[b]	0.19[c]
β_2	0.9±0.1[b]	0.29[c]
β_3	1.2±0.1[b]	0.48[c]
β_4	1.9±0.15[b]	0.48[c]

[a]From Ref. 36.
[b]From Ref. 26.
[c]From Ref. 29.

The topology of CeSb can be understood by considering the *p-f* mixing effect on the basis of the Fermi surface of LaSb.[27,28,35] The CR experiments on *RX* are interesting due to the following point. Several compounds of *RX* have large mass enhancement, although the Fermi surfaces are very simple. For example, in CeSb, which is one of the interesting strongly correlated *f*-electron systems, the effective masses m^*_{QO} are about 2 or 3 times larger than the masses (m^*_{BC}) estimated by band structure calculations as shown in Table I. If the enhancement is owing to the electron-electron interaction, m^*_{CR} are expected to be nearly equal to m^*_{BC} rather than m^*_{QO} as mentioned above. The effective masses m^*_{QO} and m^*_{BC} of LaSb, LaBi, PrSb, and GdSb reported so far are listed in Tables II–V, respectively.

The properties for each *RX* compound in this report are as follows. LaSb and LaBi are typical reference compounds for *RX*. They are simple semimetals and have no magnetic moment. GdSb is also a very simple system because Gd^{3+} with $S=7/2$ has no orbital angular momentum. GdSb is an antiferromagnet with a Néel temperature T_N of 23.4 K.[37] The magnetic structure of Gd*X* has been investigated by neutron diffraction and electron spin resonance (ESR) experiments, and the results suggest that the structure is an "easy-plane" type with the magnetic moment lying in the {111} plane.[38–40] PrSb is also a compensated semimetal. The *f*-electrons in Pr^{3+} have a nonmagnetic singlet ground state at low temperature due to the octahedral crystal electric field.[41] With increasing magnetic field, the magnetic moment is induced due to the hybridization between the ground state and excited states. Therefore, it is of interest to obtain information on the Fermi surface or the effective mass modified by a magnetic field. Some research groups measured dHvA or SdH effects on PrSb for studying the Fermi surface and estimated the effective mass so far.[30,33] CeSb is one of the interesting strongly correlated *f*-electron systems and has been studied intensively. This compound shows unusual physical properties such as the dense Kondo behavior and complicated magnetic states.[16,17,42,43] At low temperature, the spin arrangements are described by the stacking of ferromagnetic (001) planes with magnetic moments, up (↑) or down (↓), perpendicular to the planes, and the magnetic phase diagram consists of the four phases AF(↑↑↓↓), AFF2(↑↑↓↓↑↑↓), AFF1(↑↑↓), and F(↑).[43] The magnetic moment is $2.10\mu_B$ per Ce atom, similar to the saturated moment for the $|J,J_Z\rangle = |5/2,5/2\rangle$ state. The direction of the magnetic moment is strongly pinned along one of the ⟨100⟩ directions close to the applied field direction.

In order to study CR in strongly correlated *f* electron systems, we have constructed equipment which can be used

TABLE II. Summary of the effective masses for LaSb. m^*_{CR}, m^*_{QO}, and m^*_{BC} are the masses determined by the present CR measurements, the masses determined by the dHvA effect measurements taken from Ref. 19, and the masses calculated for LaSb (Ref. 20), respectively. The m^*_{QO} values in parentheses are determined by our dHvA effect measurements. m_0 is the free electron mass.

LaSb Branch	$m^*_{CR}(m_0)$ $B\|\langle 100\rangle$	$m^*_{QO}(m_0)$ $B\|\langle 100\rangle$	$m^*_{BC}(m_0)$ $B\|\langle 100\rangle$
$\alpha_\perp$	0.20	0.14[a] (0.15)	0.13[b]
$\alpha_\parallel$	-	-	0.47[b]
β	0.17	0.15[a] (0.18)	0.17[b]
γ	0.45	0.49[a] (0.50)	0.50[b]

[a]From Ref. 19.
[b]From Ref. 20.

TABLE III. Summary of the effective masses for LaBi. m^*_{CR}, m^*_{QO}, and m^*_{BC} are the masses determined by the present CR measurements, the masses determined by the dHvA effect measurements taken from Ref. 21, and the masses calculated for LaBi (Ref. 20), respectively. The m^*_{QO} values in parentheses are determined by our dHvA effect measurements. m_0 is the free electron mass.

LaBi Branch	$m^*_{CR}(m_0)$ $B\|\langle 100\rangle$	$m^*_{QO}(m_0)$ $B\|\langle 100\rangle$	$m^*_{BC}(m_0)$ $B\|\langle 100\rangle$
$\alpha_\perp$	0.33	0.4[a] (0.28)	0.25[b]
$\alpha_\parallel$	-	-	0.69[b]
β	0.20	0.18[a] (0.18)	0.13[b]
γ	0.65	0.63[a] (0.63)	0.62[b]

[a]From Ref. 21.
[b]From Ref. 20.

TABLE IV. Summary of the effective masses for PrSb. m^*_{CR} and m^*_{QO} are the masses determined by the present CR measurements and the masses determined by the dHvA effect measurements taken from Ref. 30, respectively. The m^*_{CR} values in parentheses denote that the branches are not determined experimentally. m_0 is the free electron mass.

PrSb Branch	$m^*_{CR}(m_0)$ $B\|\langle 100\rangle$	$m^*_{QO}(m_0)$ $B\|\langle 100\rangle$	$m^*_{QO}(m_0)$ $B\|\langle 110\rangle$
$\alpha_\perp$	(0.25)	0.19[a]	-
$\alpha_\parallel$	-	-	-
β	(0.3)	-	0.22[a]
γ	(0.53)	0.40[a]	-

[a]From Ref. 30.

for both ESR and CR in high frequencies up to 190 GHz and high magnetic fields up to 15 T. This equipment consists of a vector network analyzer and a resonant cavity, which enable us to clearly detect the signals even for relatively high conductive compounds. In addition, we prepared high-quality single crystals of LaSb, LaBi, CeSb, and GdSb. A high-quality single crystal of PrSb was also prepared by Canfield and Cunningham at Ames Laboratory, Iowa State University. The typical residual resistivity ρ_0 and residual resistivity ratio (RRR) of the crystals are $\sim 0.1\ \mu\Omega$ cm and ~ 500, respectively, which showed that the crystals were several times higher in quality than crystals in previous reports.

Using these single crystals, we successfully observed CR absorption lines.[44–49] These lines show the linear relation between frequency and magnetic field. In addition to them, we have also observed "anomalous" cyclotron resonances lines that show nonlinear behavior with respect to magnetic field in the higher-field region. The anomalous behavior can be explained by Doppler-shifted cyclotron resonance (DSCR) with Alfvén waves in the semimetals *RX*.[50] The purpose of this paper is to reexamine our recent results of CR and DSCR first observed in *RX* and to compare m^*_{CR} with m^*_{QO} and m^*_{BC} systematically. And then, we discuss the origin of mass enhancement in this system. In this paper, we also describe the experimental details such as the sample preparation and characterization and the development of measurement system.

TABLE V. Summary of the effective masses for GdSb. m^*_{CR} and m^*_{QO} are the masses determined by the present CR measurements and the masses determined by the dHvA effect measurements (Refs. 30 and 34), respectively. The m^*_{CR} values in parentheses denote that the branches are not determined experimetally. m_0 is the free electron mass.

GdSb Branch	$m^*_{CR}(m_0)$ $B\|\langle 100\rangle$	$m^*_{QO}(m_0)$ $B\|\langle 100\rangle$	$m^*_{QO}(m_0)$ $B\|\langle 111\rangle$
$\alpha_\perp$	-	0.14[a]	0.24[b]
$\alpha_\parallel$	-	0.52[a]	0.24[b]
β	(0.26)	0.23[a]	0.19[b]
γ	(0.50)	-	0.38[b]

[a]From Ref. 30.
[b]From Ref. 34.

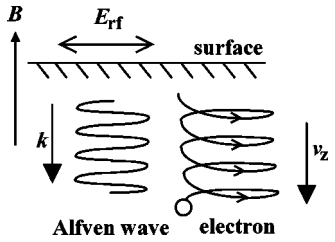

FIG. 1. Schematic picture of an electron motion and Alfvén wave propagation.

II. CR AND DSCR RESONANCE CONDITIONS IN SEMIMETALS

In this section, we summarize the resonance conditions of CR and DSCR in semimetals, which is necessary to analyze our CR and DSCR data. In general, cyclotron resonance occurs when the microwave frequency ω coincides with the cyclotron frequency ω_c given by

$$\omega_c = \frac{eB}{m^*_{CR}}, \tag{1}$$

where e and B are the charge of the carrier and magnetic field, respectively. We can determine m^*_{CR} using this relation. However, in metals or semimetals, the microwave is very rapidly attenuated due to the skin effect when it penetrates into the bulk crystal. In these cases, the CR spectrum depends on the relation between the magnetic field direction and the sample surface. When the magnetic field is parallel to the sample surface, the Azbel-Kaner type cyclotron resonance is observed at $\omega = n\omega_c$, where n is an integer.[51] On the other hand, when the magnetic field is perpendicular to the sample surface, only carriers within the skin depth couple with the microwave at the condition $\omega = \omega_c$. Most of carriers are below the skin depth, and they cannot couple with the microwave, penetrating only near the surface of the material.

It is known, however, that the electromagnetic wave of the frequency satisfying $\omega \ll \omega_c$ can propagate inside the bulk of metal or semimetal in a high magnetic field if the sample quality is very high such as a magnetoplasma wave.[52] For a compensated semimetal such as *RX*, this wave is called an Alfvén wave. In this case, there is a possibility that the carriers couple with a microwave even in a bulk. In the B direction perpendicular to both the sample surface and the rf electric field E_{rf} as shown in Fig. 1, the Alfvén wave propagates along the direction of B (z direction). A carrier that has a velocity component v_z along the z direction couples with the rf field of the Alfvén wave with the Doppler-shifted frequency $\omega \pm kv_z$, where k is the wave number of the Alfvén wave. In this case, DSCR occurs when the cyclotron frequency ω_c coincides with $\omega \pm kv_z$. The dispersion relation of isotropic Alfvén waves under the conditions $\omega_c\tau \gg 1$ and $\omega \ll \omega_c$ is given by

$$k^2 = \frac{\mu \Sigma_j n_j m_j}{B^2}\omega^2 = \frac{\lambda}{B^2}\omega^2, \tag{2}$$

where τ is the relaxation time of the carrier, μ the magnetic susceptibility, n_j the density of the jth carrier, and m_j its

TABLE VI. ρ_0 and RRR of the most high-quality single crystal for each compounds.

	$\rho_0(\mu\Omega\,\mathrm{cm})$	RRR
LaSb	0.13	490
LaBi	-	-
CeSb	~0.3	~500
PrSb	-	514
GdSb	~0.1	~500

mass.[52,53] Substituting Eq. (2) into the resonance condition, we obtain the magnetic field dependence of the resonance frequency ω' for DSCR:

$$\omega' = \frac{\omega_c}{1 + (v_z\sqrt{\lambda}/B)}. \tag{3}$$

Here, we adopt the condition of $\omega_c = \omega + kv_z$. The other condition $\omega_c = \omega - kv_z$ means that the resonance field shifts to the lower-field side and the Alvfén wave with this frequency cannot propagate because the condition $\omega \ll \omega_c$ is not satisfied.

In DSCR measurements, a detected anomaly is mainly due to the carriers around the edge of the Fermi surface in which the carrier has the maximum Fermi velocity along the B direction.[52,53] Therefore, m^*_{CR} related to DSCR measurements is generally different from that of CR measurements. However, if the Fermi surface is a sphere or ellipsoid, all cyclotron orbits at a fixed direction have the same m^*_{CR} value. In this paper, we approximate the α, β, and γ branches of *RX* to be spheres or ellipsoids for simplification and we use the m^*_{CR} values determined by CR measurements for analysis of DCSR signals. In this approximation, the calculation of λ is also very simplified.

It is noted that the resonance condition of DSCR depends both on the effective mass and on the Fermi velocity v_F, which means that we can estimate v_F from DSCR measurements directly if the effective mass parameters are completely determined.

III. EXPERIMENTAL DETAILS

A. Sample preparation and characterization

The high-quality single crystals of LaSb, LaBi, CeSb, and GdSb were synthesized in tungsten crucibles by the Bridgman method. Rare-earth metals of 99.99% purity and pnictogen metals of 99.9999% purity were used. The PrSb single crystal was prepared by Canfield and Cunningham at Ames Laboratory, Iowa State University.[48] The electric resistivity was measured for characterization. ρ_0 and the RRR of the most high-quality single crystal are listed in Table VI for each compound. By using the free electron model with typical values of the resistivity ρ ($0.1\ \mu\Omega\,\mathrm{cm}$), the effective mass m^* ($\sim 0.5m_0$), and the density of carriers n ($\sim 4\times10^{26}\ m^{-3}$) for *RX*, the relaxation time τ is estimated to be 4×10^{-11} sec. Considering the typical frequency of our system (~72 GHz), the CR condition $\omega\tau$ (~ 20) $\gg 1$ is sufficiently satisfied.

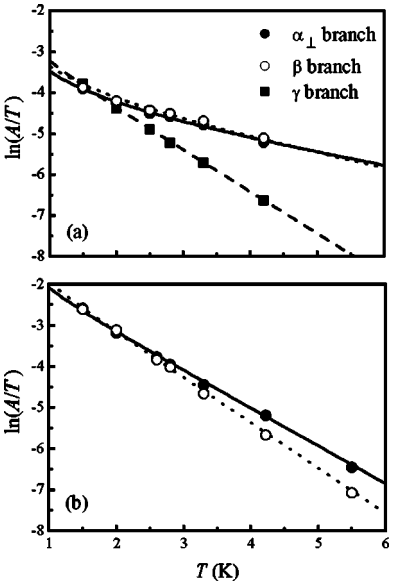

FIG. 2. Temperature dependence of dHvA amplitudes for LaSb in magnetic fields B parallel to the ⟨100⟩ direction. The fast Fourier transform (FFT) analysis has been performed in the magnetic field range from 6 to 9 T for (a) and in the magnetic field range from 2 to 3 T for (b). The solid line, the dotted line, and the dashed line are the calculated temperature dependence of dHvA amplitudes, which correspond to m^*_{QO} of $0.15m_0$, $0.18m_0$, and $0.50m_0$, respectively.

Using these LaSb and LaBi single crystals, we also measured dHvA effects by a standard field modulation technique in order to compare the results of our high-quality single crystals with the previous reports. Figure 2 shows the temperature T dependence of the dHvA amplitudes A for LaSb in magnetic fields B parallel to the ⟨100⟩ direction. The FFT analysis has been performed in the magnetic field range from 6 to 9 T for (a) and from 2 to 3 T for (b), respectively. The lines in this figure are calculated using a relation of $\ln(A/T) = \ln[\mathrm{const}/\sinh(14.69m^*_{QO}T/B)]$. In the higher-field region (a), the $\alpha_\perp$, β, and γ branches are clearly observed in a wide temperature range, and the m^*_{QO} values are estimated to be $0.2m_0$ for the $\alpha_\perp$ and β branches and to be $0.50m_0$ for the γ branch. However, in this region, it is difficult to determine the small effective masses for the $\alpha_\perp$ and β branches precisely, because the decrease of the amplitude A is very weak in the higher-field region, so that we estimate the effective masses for the $\alpha_\perp$ and β branches at the lower-field region (b). As seen in Fig. 2(b), the reduction of the amplitude A for the β branch is larger than that for the $\alpha_\perp$ branch in increasing temperature. Then it is obvious that m^*_{QO} for the β branch is larger than that for the $\alpha_\perp$ branch. The m^*_{QO} values are estimated to be about $0.15m_0$ and $0.18m_0$ for the $\alpha_\perp$ and β branches, respectively.

Figure 3 shows the temperature dependence of the dHvA amplitudes A for LaBi in magnetic fields B parallel to the ⟨100⟩ direction. The FFT analysis has been performed in the magnetic field range from 6 to 9 T for (a) and from 3 to 4 T for (b), respectively. The m^*_{QO} values for LaBi are estimated to be $0.28m_0$, $0.18m_0$, and $0.63m_0$ for the $\alpha_\perp$, β, and γ branches, respectively, in the same way as for LaSb.

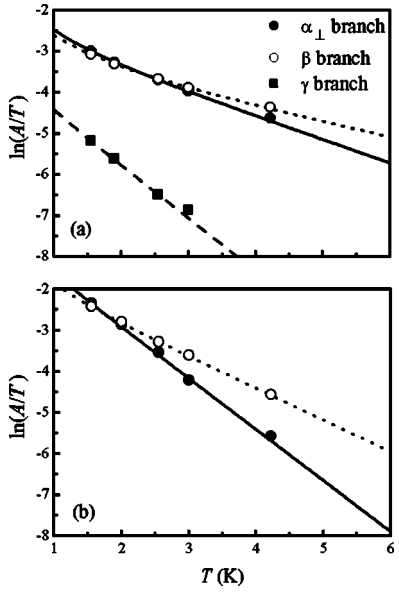

FIG. 3. Temperature dependence of dHvA amplitudes for LaBi in magnetic fields B parallel to the ⟨100⟩ direction. The FFT analysis has been performed in the magnetic field range from 6 to 9 T for (a) and in the magnetic field range from 2 to 3 T for (b). The solid line, the dotted line, and the dashed line are the calculated temperature dependence of dHvA amplitudes, which correspond to m^*_{QO} of $0.28m_0$, $0.18m_0$, and $0.63m_0$, respectively.

The obtained m^*_{QO} are listed in Tables II and III, and these values are quite consistent with those in the previous reports. This result shows that the Fermi surface topology and m^*_{QO} have no sample dependence.

B. Cyclotron resonance measurements

Figure 4 shows the schematic drawing of the CR measurement system. This equipment consists of a vector network analyzer (AB Millimetre, Co. and Ltd.) and a resonant cavity. The vector network analyzer acts a tunable source and detector of the millimeter-wave radiation. Because the frequency can be changed continuously, it is easy to tune the frequency to the resonance frequency of the cavity. In addition, the vector network analyzer can detect the amplitude and phase shift of the microwave simultaneously. Therefore, the vector network analyzer is very useful for ESR and CR measurements, and several other groups have developed unique techniques using the vector network analyzer.[3–5,54,55] We made the cavity using oxygen-free copper in such a way that the resonant frequencies for TE_{011} and TE_{012} are 58 and 72 GHz, respectively. We refer the reader to a series of excellent articles on the cavity perturbation technique.[3,55,56] By using a variable temperature insert (VTI) and temperature controller, high-temperature stability is realized. Temperature stability is important, because the cavity is very sensitive to a change of temperature.

The single crystal was cut into small plates with a size of $1\times1\times0.2$ mm^3 along the (001) plane. Cyclotron resonance measurements for the single crystal have been performed in the frequency region from 50 to 190 GHz in magnetic fields

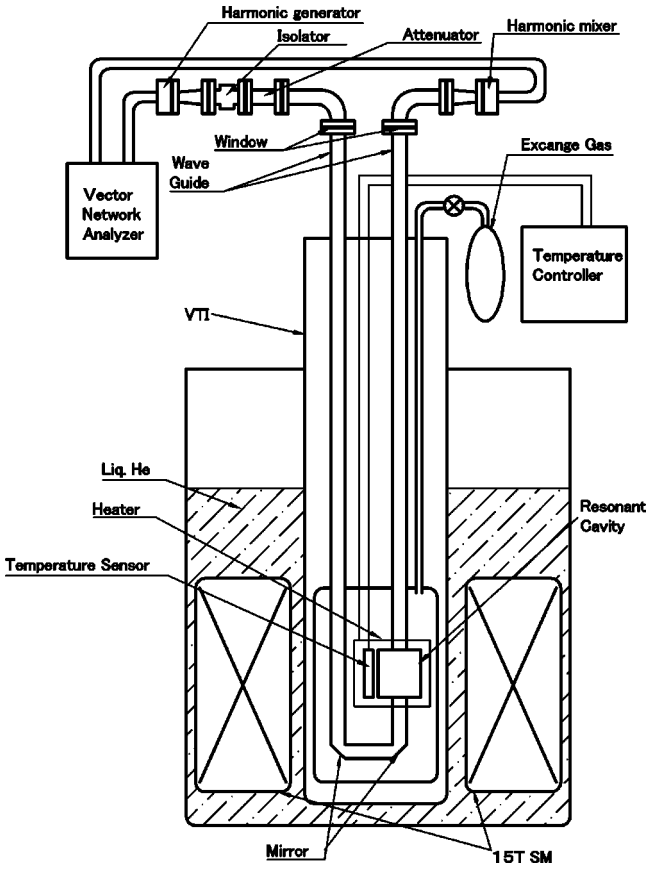

FIG. 4. The schematic picture of the CR measurement system.

up to 14 T using a superconducting magnet (SM) at the High Field Laboratory for Superconducting Materials, Institute for Materials Research, Tohoku University. In the cavity, the sample was placed at the top of the pillar, where the rf electric field of the microwave is nearly maximum for the TE_{011} or TE_{012} mode. We avoided the position where the rf electric field of the microwave is maximum, because the Q value was largely reduced. Typical Q values of the empty and loaded cavities were about 20 000 and 10 000 at 4.2 K for the TE_{011} mode, respectively. The applied magnetic field B was perpendicular to the rf electric fields of the TE modes. The angular dependence was measured by changing the angle of the pillar. In this work, we performed CR measurements using other TE or TM modes at the same sample position, because the sample experiences the components of the rf electric fields and the signal can be detected.

Figure 5 shows the cavity transmission amplitude and phase shift for LaSb at 72.7 GHz and 1.6 K in magnetic fields parallel to the [001] direction. We can see four absorption lines labeled as A–D, while the transmission amplitude decreases with increasing the magnetic field. This decrease seems to be due to the increase of the transversal magnetoresistance. It is very complicated to calculate the entire shape of the spectrum, because the system is in the anomalous skin effect regime. In this study, however, we focus only on the resonance field, which is concerned with the effective mass. In Fig. 5, the vertical dashed lines indicate the determined resonance fields. Here, we can determine the resonance fields

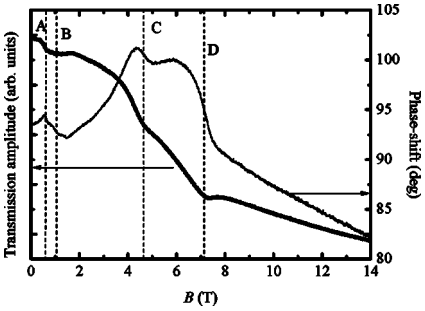

FIG. 5. Cavity transmission amplitude and phase shift for LaSb at 72.7 GHz and 1.6 K in magnetic fields parallel to the [001] direction. The thick and thin lines show the amplitude and phase shift, respectively.

more precisely by analyzing both the amplitude and phase shift. In this study, we also confirmed that the spectrum is independent of the sample dimension by using several samples cut into various sizes.

Figure 6 shows the cavity transmissions for three typical single crystals of LaSb at 1.6 K and about 72 GHz (TE_{012} mode) in magnetic fields B parallel to the [001] direction. The three crystals are labeled as 3N, 4N#1, and 4N#2, respectively. The 99.9% pure crystal was synthesized from La metal of 99.9% purity and Sb metal of 99.9999% purity. Both the 4N#1 and 4N#2 crystals were synthesized from La metal of 99.99% purity and Sb metal of 99.9999%, and the RRR's for 4N#1 and 4N#2 are 100 and 490, respectively. In Fig. 6, we can see the importance of the sample quality for CR measurements. For the spectrum of the 99.9% pure sample, one small absorption line can be seen at about 2.5 T, which corresponds to "$g=2$." This absorption line is considered to be a magnetic resonance due to magnetic impurities such as Gd^{3+}. There is no signal in the lower-field region; that is, no CR signal is observed in the 99.9% pure sample. On the other hand, in the high-quality 4N#2 sample, two clear absorption lines are observed. These absorption lines are the cyclotron resonances of carriers in LaSb as discussed in Sec. IV. These resonance fields are 0.53 and 1.2 T, and we can estimate m^*_{CR} to be $0.20m_0$ and $0.5m_0$, respectively. The resonance fields can be determined more precisely by using a higher frequency, because it gives a better CR condition $\omega\tau \gg 1$. The 4N#1 is also a high-quality single crystal of which the RRR is about 100. However, this quality is not sufficient for CR measurements. Although a very broad CR signal is observed at about 0.8 T, the broad line should consist of the two (or three) CR signals and it is difficult to estimate m^*_{CR} precisely in this spectra. One could separate the broad line into the CR signals, using a much higher frequency. However, such a high-frequency measurement with high sensitivity is very difficult. In the following section, we only deal with the results of the best quality samples.

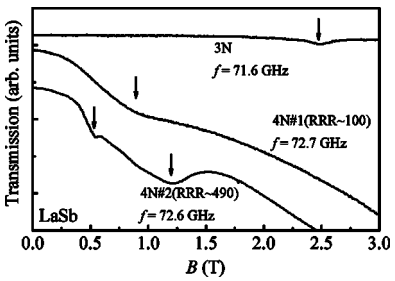

FIG. 6. Cavity transmissions for three typical single crystals (3N, 4N#1, and 4N#2) of LaSb at 1.6 K and about 72 GHz in magnetic fields B parallel to the [001] direction. The resonance features are indicated by the arrows.

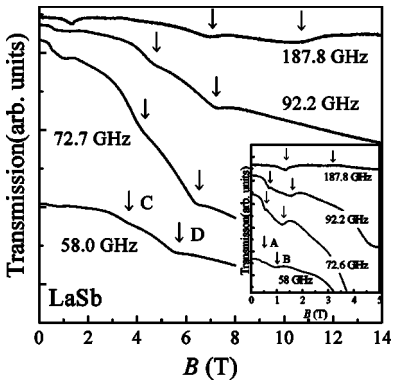

FIG. 7. Cavity transmissions for LaSb for various frequencies at 1.6 K in magnetic fields parallel to the [001] direction. The inset shows the spectra at the lower-field region. The arrows indicate the resonance features.

IV. RESULTS AND DISCUSSION

A. Cyclotron resonance in a simple semimetal LaSb

Figure 7 shows the cavity transmissions for LaSb for various frequencies at 1.6 K in magnetic fields B parallel to the [001] direction. Here, the B direction is perpendicular to the sample surface, which is not the Azbel-Kaner configuration. The inset of Fig. 7 shows the spectra at the lower-field region. In Fig. 7 and the inset, we can see four absorption lines at each frequency, and these absorption lines are labeled as A–D, respectively. Figure 8 shows the cavity transmission amplitude and the phase shift for LaSb at around the absorption line A at 187.8 GHz. In this figure, we can see a small dip at the lower-field side of the absorption line A. The dip is considered to be another absorption line, because the phase

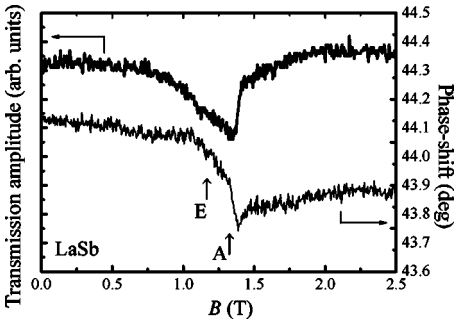

FIG. 8. Cavity transmission amplitude and phase shift for LaSb at 187.8 GHz and 1.6 K in magnetic fields parallel to the [001] direction. The thick and thin lines show the amplitude and phase shift, respectively.

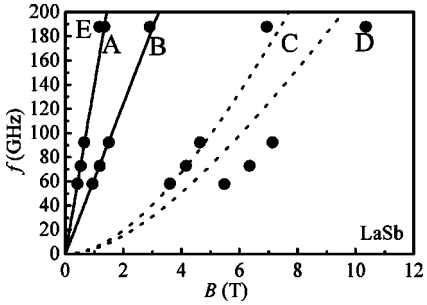

FIG. 9. Frequency-field diagram of LaSb at 1.6 K for $B\|[001]$. The solid lines correspond to the CR liner relations with the m^*_{CR} values of $0.20m_0$ and $0.45m_0$, respectively. The dotted lines are calculated from Eq. (3) and correspond to the edges of the γ branch and $\alpha_\|$ branch, respectively.

shift also changes at the dip. The dip is labeled as *E*.

Figure 9 shows the frequency-field diagram of LaSb for the [001] direction. From the liner relation of Eq. (1), m^*_{CR} is determined to be $0.20m_0$ and $0.45m_0$, respectively. The resonance point of *E* corresponds to $0.17m_0$, although the frequency dependence cannot be obtained. On the other hand, the resonance frequencies of *C* and *D* show nonlinear behavior with respect to the magnetic field. This anomalous behavior of the *C* and *D* lines is explained by DSCR as discussed later.

Figure 10 shows the cavity transmissions for LaSb for various magnetic field directions at about 70 GHz (TE_{012} mode). Here, Θ is the angle in degrees between the magnetic field and the [001] direction in the (010) plane. Two or three absorption lines are observed at each Θ. In Fig. 10, we can also see Azbel-Kaner cyclotron resonance (AKCR) at $\Theta=90°$ below 2 T. Here, the field was parallel to the (001) plane—that is, parallel to the sample surface. In the Azbel-Kaner configuration, the resonance occurs when $\omega=n\omega_c$ where *n* is an integer.[51] From the AKCR spectrum, m^*_{CR} is

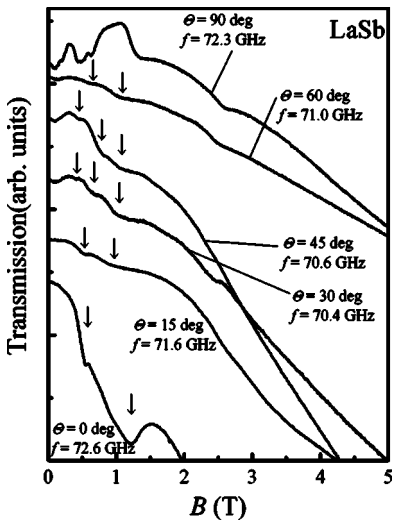

FIG. 10. Cavity transmissions for LaSb for various magnetic field directions at about 70 GHz and at 1.6 K. Θ is the angle in degrees between the magnetic field and the [001] direction in the (010) plane. The arrows indicate the resonance features.

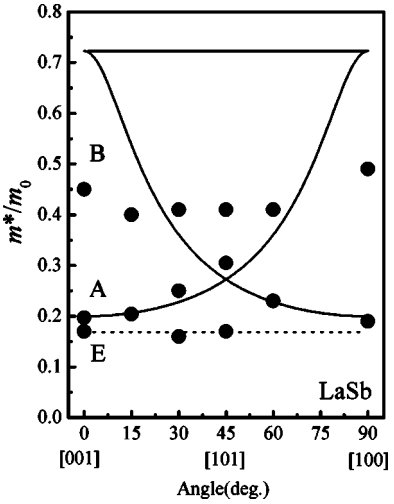

FIG. 11. Angular dependence of m^*_{CR} for LaSb estimated from the CR experiments (solid circles). The solid lines and the dotted line indicate the calculated angular dependence of m^*_{CR} for the α branch and β branch, respectively.

estimated to be $0.2m_0$ and $0.5m_0$, respectively. These values are consistent with the result at $\Theta=0°$, where *B* is perpendicular to the sample surface. Figure 11 shows the angular dependence of m^*_{CR} from the [001] direction to the [100] direction. Here, we discuss the branches of *A*, *B*, and *E*. As seen in Fig. 11, the m^*_{CR} value of *A*, which is $0.20m_0$ at $\Theta=0°$, increases with increasing Θ from 0° to 45°. In the Fermi surface of LaSb, only the cyclotron effective mass of the α branch of which longitudinal axis is parallel to the [001] direction is expected to increase with increasing Θ from the [001] direction to the [101] direction. Therefore, the absorption line *A* is considered to be the α branch. Using an ellipsoidal Fermi surface model, the angular dependence of m^*_{CR} is given by

$$\frac{1}{(m^*_{CR})^2}=\frac{\cos^2\theta}{m_\perp^2}+\frac{\sin^2\theta}{m_\|^2}, \tag{4}$$

where $m_\perp$ and $m_\|$ are the cyclotron mass for the plane perpendicular to the longitudinal axis of the spheroid and for a plane including the axis, respectively, and θ is the angle from the axis. The solid lines in Fig. 11 correspond to the three equivalent ellipsoids of the α branch and are calculated using parameters $m_\perp=0.20m_0$ and $m_\|=0.72m_0$. Here, we assume that mass ratio $m_\perp/m_\|$ is equal to that of the band structure calculation ($m_\perp=0.13m_0$ and $m_\|=0.47m_0$).[20] As seen in Fig. 11, the agreement between the experimental m^*_{CR} of *A* and the calculated one is fairly good from the [001] direction to the [101] direction. Therefore, the resonance *A* originates from the cyclotron motion of the carriers in the α branch. On the other hand, the resonance *B* seems to originate from the γ branch for the following reasons. m^*_{CR} for *B* is very close to m^*_{QO} for the γ branch. In addition, the angular dependence is similar to that of the extremal cross-sectional area of the γ branch.[19] The resonance *E* seems to be the β branch, which shows no angular dependence. In Fig. 11, the dotted line is

an expected angular dependence of m^*_{CR} for the β branch. In Table II, the obtained m^*_{CR} are summarized.

B. Doppler-shifted cyclotorn resonance

As seen in Fig. 9 the resonance frequencies of *C* and *D* show nonlinear behavior with respect to the magnetic field. In addition, their resonance fields are fairly high. That is, if these *C* and *D* resonances are assumed to be CR lines, the effective masses are estimated to be over $1.0m_0$, which are much larger than the expected masses in LaSb. Then it is impossible to explain such features by the normal CR relation. The single crystal of LaSb used in the present measurements is quite high quality, so that there is a possibility that the Alfvén wave propagates inside the crystal and DSCR can be observed. The resonance condition of Eq. (3) means that the DSCR resonance field should be higher than the "normal" CR resonance field and the resonance frequency of DSCR should be nonlinear with respect to *B* except for the region $B \gg v_z\sqrt{\lambda}$. That is, the qualitative features of the DSCR resonance condition are consistent with those of *C* and *D*. In order to investigate the *C* and *D* lines quantitatively, we have to determine λ in Eq. (3) more carefully according to the empirical data of this crystal. The Fermi surface of LaSb consists of the three branches α, β, and γ. For simplification, we assume the γ branch to be a sphere. Then the dispersion relation of the Alfvén waves in LaSb is written as

$$k^2 = \frac{\mu[(2/3)n_\alpha m_t + (1/3)n_\alpha m_l + n_\beta m_\beta + n_\gamma m_\gamma]}{B^2}\omega^2 = \frac{\lambda}{B^2}\omega^2, \tag{5}$$

where n_α, n_β, and n_γ are the densities of the carriers in the α, β, and γ branches; m_t and m_l are the transverse and longitudinal masses of the α branch; m_β and m_γ are the effective mass of the β and γ branches, respectively. In DSCR measurements, a detected anomaly is mainly due to the carriers around the edge of the Fermi surface in which the carrier has the maximum Fermi velocity along the *B* direction. LaSb has four edges of the Fermi surface for the [001] direction—that is, the edges of the β branch, the γ branch, and the two types of the α branch ($\alpha_\perp$, the longitudinal axis of the spheroid is parallel to the [001] direction; $\alpha_\parallel$, the axis is perpendicular to the [001] direction). The dotted lines in Fig. 9 are calculated from Eq. (3) using the parameters obtained experimentally for the edges of the γ and $\alpha_\parallel$ branches, respectively. The agreement between the experimental data of *C* and *D* and the calculated lines is reasonably good. Therefore, we conclude that the *C* and *D* lines are due to DSCR of the carriers at the edges of the γ and $\alpha_\parallel$ branches, respectively. Here, the carrier densities n_α ($=2.0\times10^{26}$), n_β ($=0.5\times10^{26}$), and n_γ ($=1.5\times10^{26}\ m^{-3}$) are taken from Ref. 30 and the effective-mass parameters m_t ($=0.20m_0$), m_β ($=0.17m_0$), and m_γ ($=0.45m_0$) are deduced from the CR measurement. Unfortunately, m_l is not determined experimentally, so that we use $m_l=2.6m_0$, assuming that the mass ratio $m_t/m_l(=0.077)$ is equal to that of the band structure calculation ($m_t=0.13m_0$ and $\sqrt{m_t m_l}=0.47m_0$).[20] Since the Fermi velocities v_F at the edges also have not been reported, v_F ($=0.46\times10^6$ for the $\alpha_\parallel$ branch and 0.6×10^6 m/s for the γ branch) are roughly estimated from the results of the dHvA measurements using the relation $v_F=\hbar k_F/m^*$.[19,30]

In this work, the DSCR signals of the β and $\alpha_\perp$ branches have not been observed. Since Alfvén waves are more strongly attenuated in the lower-field region, the DSCR signal that shifts to the highest field would be observed most clearly. In the case of LaSb, according to our estimation the resonance field of the $\alpha_\parallel$ branch is largest and the resonance fields of the β and $\alpha_\perp$ branches are smaller than those of the γ and $\alpha_\parallel$ branches at a fixed frequency. Therefore, the DCSR signal of the $\alpha_\parallel$ branch can be observed most clearly. In contrast, it may be more difficult to observe the DSCR signals of the β and $\alpha_\perp$ branches.

The transmission of magnetoplasma waves requires a quite high-quality sample, so that there is no report of DSCR except for pure metals or semimetals such as Cu, Na, and Bi, as far as we know. In this study, we prepared the quite high-quality single crystals, and then we observed DSCR including the nonlinear behavior on the frequency-field diagram. There is a possibility that the nonlinear behavior is due to the nonparabolic band effect. In the case of LaSb, however, the individual resonance positions correspond to $(1-3)m_0$, which is much larger than the masses expected from the band structure calculation and the dHvA effect measurements. Although we have also performed dHvA effect measurements for our crystals as described in Sec. II, we could not find other branches with large effective masses. And our dHvA measurements are quite consistent with the previous reports. Therefore, we believe that the resonances are DSCR.

C. Cyclotron resonance in LaBi, PrSb, and GdSb

In this study, we have also observed CR and DSCR in LaBi, PrSb, and GdSb.[45,48,49,57] These compounds have the same Fermi surface topology as LaSb. In particular, LaBi is also a simple semimetal as well as is LaSb. The m^*_{CR} values for LaBi are estimated to be $0.20m_0$, $0.33m_0$, and $0.65m_0$, for the β, $\alpha_\perp$, and γ branches, respectively,[45,57] and they are reasonably consistent with m^*_{QO} and m^*_{BC} as shown in Table III. The effective masses of LaBi are somewhat larger than those of LaSb. This difference is considered to be due to the difference in the curvature of the band which arises from changing Sb into Bi. These results show that the effective masses of both LaSb and LaBi are dominated by the band structure.

For PrSb, m^*_{CR} are determined to be $0.25m_0$, $0.3m_0$, and $0.53m_0$, respectively.[48] On the other hand, the cyclotron effective masses m^*_{QO} estimated from the acoustic dHvA measurements by Settai[30] are reported with the values of $0.19m_0$, $0.22m_0$, and $0.40m_0$ for the $\alpha_\perp$, β, and γ branches, respectively, as shown in Table IV. Here, m^*_{QO} for the $\alpha_\perp$ and γ branches were estimated in the magnetic fields parallel to the $\langle100\rangle$ direction. Although m^*_{QO} for the β branch was estimated in the magnetic fields parallel to the $\langle110\rangle$ direction, the β branch is expected to have no angular dependence. In our CR measurements the obtained m^*_{CR} are about 30% larger than m^*_{QO}, on the assumption that m^*_{CR} with the values of

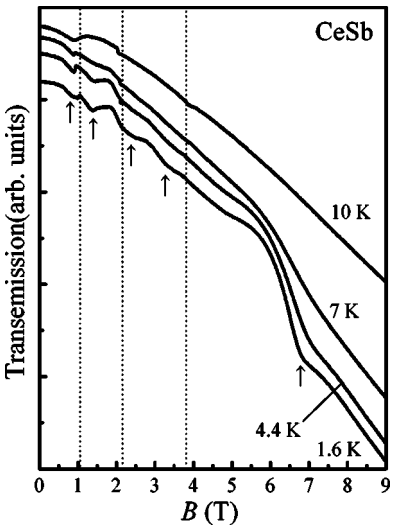

FIG. 12. Cavity transmissions for CeSb at various temperatures at 72.5 GHz in magnetic fields parallel to the [001] direction. The vertical dotted lines indicate the magnetic transition fields at 1.6 K. The arrows indicate the resonance features.

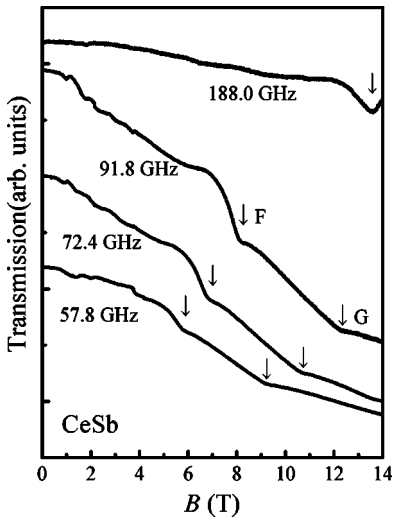

FIG. 13. Cavity transmissions for CeSb at various frequencies at 1.6 K in magnetic fields parallel to the [001] direction. The arrows indicate the resonance features.

$0.25m_0$, $0.3m_0$, and $0.53m_0$ correspond to the $\alpha_\perp$, β, and γ branches, respectively. The estimated m^*_{CR} are listed in Table IV.

In GdSb, the antiferromagnetic resonance (AFMR) is observed at low temperatures. The magnetic resonance signals of Gd^{3+} are very strong due to its large magnetic moment, so that the signals are detected whenever the sample experiences the components of the rf magnetic fields. In addition to AFMR, we have observed two CR signals and m^*_{CR} are determined to be $0.26m_0$ and $0.50m_0$, respectively.[49] These values are reasonably consistent with the m^*_{QO} values of GdSb and the values of the nonmagnetic reference compound LaSb as seen in Tables II and V.

D. Cyclotron resonance in a strongly correlated *f*-electron system CeSb

Figure 12 shows the cavity transmissions for CeSb at various temperatures from 1.6 K to 10 K at 72.5 GHz in magnetic fields B parallel to the [001] direction. Here, the B direction is perpendicular to the sample surface. The vertical dotted lines in this figure indicate the magnetic phase transition fields at 1.6 K. At these fields, we observe small anomalies that are due to the changes of the magnetic permeability or the electric resistivity with the transitions. As shown in Fig. 12, five absorption lines are observed at 1.6 K, and their characteristic features are that they become broader with increasing temperature from 1.6 K and undetectable above 10 K, independent of the magnetic phase diagram.[43] These findings indicate that the observed absorption lines do not originate from antiferromagnetic resonances of the magnetic moment due to $4f$ electrons in CeSb. On the other hand, CR absorption lines in a metal or semimetal rapidly vanish with increasing temperature. Therefore, we believe that the observed absorption lines are the cyclotron resonances of the carriers in CeSb.

In Fig. 12, the large absorption line at 6.8 T is considered to be DSCR and the other absorption lines are considered to be CR. This distinction between CR and DSCR is derived from the frequency dependence of the resonance field. Figure 13 shows the cavity transmissions for CeSb for various frequencies at 1.6 K in magnetic fields B parallel to the [001] direction. We can see two large absorption lines which are labeled as F and G, respectively. The absorption line F corresponds to the large absorption line at 6.8 T in Fig. 12. These two lines shift to the higher-field side with increasing frequency. Figure 14 shows the frequency-field diagram for the absorption lines F and G for CeSb in magnetic fields B parallel to the [001] direction. The resonance points are not indicated by any straight lines crossing the origin, but are indicated by the dotted lines in Fig. 14. These lines are calculated by the DSCR resonance condition, Eq. (3). Therefore, the absorption lines F and G are considered to be DSCR of the carriers in CeSb.

Figure 15 shows the cavity transmissions for CeSb for various frequencies at 1.6 K at the lower-field region. The absorption lines shift with changing the frequency. Figure 16 shows the cavity transmission amplitude and phase shift for CeSb at 188.0 GHz at 1.6 K in magnetic fields parallel to the [001] direction. In addition to the DSCR signal F, four ab-

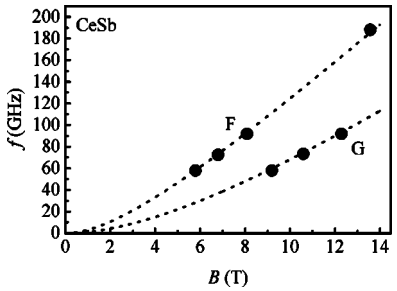

FIG. 14. Frequency-field diagram of the resonances F and G for CeSb at 1.6 K for $B\|[001]$. The dotted lines are the DSCR relations calculated from Eq. (3).

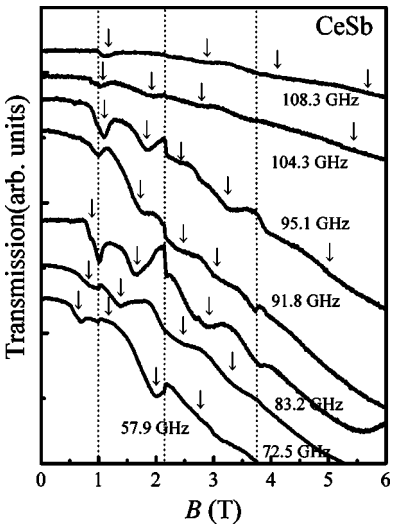

FIG. 15. Cavity transmissions for CeSb for various frequencies at 1.6 K at the lower-field region. The vertical dotted lines indicate the magnetic transition fields at 1.6 K. The arrows indicate the resonance features.

sorption lines are observed. From these spectra, the frequency-field diagram of CR for CeSb is obtained as Fig. 17 for the [001] direction at 1.6 K. The CR data in Fig. 17 are on the straight lines crossing the origin. The vertical dotted lines indicate the magnetic phase transition fields at 1.6 K, and the four magnetic phases are labeled as AF, AFF2, AFF1, and F, respectively. Here, some absorption lines that observed in a certain phase cannot be observed in other phases, because the Fermi surface of CeSb changes at each transition fields. Therefore, m^*_{CR} should be estimated in each phase independently.

In the AF phase, there is only one branch and m^*_{CR} is determined to be $0.30m_0$. However, we cannot compare m^*_{CR} with m^*_{QO} in this phase, because dHvA measurements have not been reported yet in this phase. In the AFF2 phase, we have observed four branches and m^*_{CR} are determined to be $0.21m_0$, $0.26m_0$, $0.54m_0$, and $0.9m_0$, respectively. As shown in Table I, the dHvA measurements in this phase are reported

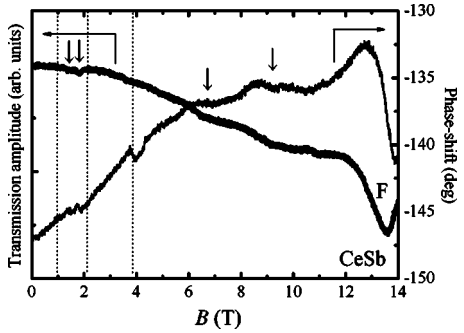

FIG. 16. Cavity transmission amplitude and phase shift for CeSb at 188.0 GHz at 1.6 K in magnetic fields parallel to the [001] direction. The thick and thin lines show the amplitude and phase shift, respectively. The vertical dotted lines indicate the magnetic transition fields at 1.6 K. The arrows indicate the resonance features.

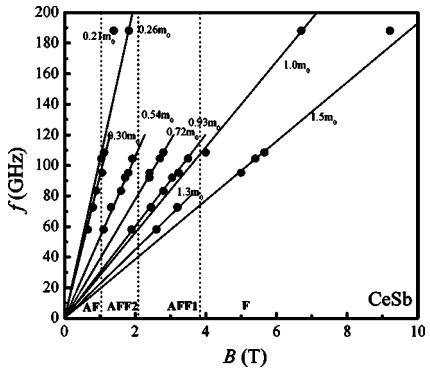

FIG. 17. Frequency-field diagram of CeSb at 1.6 K for $B\|[001]$. The data for F and G are not shown. The vertical dotted lines indicate the magnetic transition fields at 1.6 K.

with m^*_{QO} of $0.2m_0$ and $0.3m_0$ for the [001] direction. The m^*_{CR} values of $0.21m_0$ and $0.26m_0$ in our measurements are consistent with the values of m^*_{QO}. On the other hand, m^*_{CR} of $0.54m_0$ and $0.9m_0$ are much larger than m^*_{QO} and this result is inconsistent with the Kohn's theorem. There should be some other branches, but they have not yet been observed by dHvA measurements. It is necessary to investigate this phase by dHvA measurements using a high-quality single crystal. In the AFF1 phase, three branches are observed and m^*_{CR} are determined to be $0.72m_0$, $0.93m_0$, and $1.3m_0$, respectively. In the F phase, m^*_{CR} are determined to be $1.0m_0$ and $1.5m_0$.

In the AFF1 and F phases, the Fermi surfaces have been investigated by the dHvA measurements and the band structure calculation completely and all branches probably have been reported in these phases. Therefore, a branch observed in our CR measurements of these phases should correspond to the appropriate branch reported in the dHvA measurements and the band structure calculation. In our CR measurements, m^*_{CR} of $1.3m_0$ and $1.5m_0$ are the largest masses in the AFF1 and F phases, respectively. Therefore, it is a reasonable assumption that m^*_{CR} of $1.3m_0$ and $1.5m_0$ correspond to the β_4' and β_4 branches, respectively. On this assumption, m^*_{CR} are smaller than m^*_{QO} and this results does not conflict with the Kohn's theorem. However, m^*_{CR} of $1.3m_0$ and $1.5m_0$ are quite larger than m^*_{BC} and the values of m^*_{CR} are close to those of m^*_{QO} rather than m^*_{BC}. This fact shows that m^*_{CR}, as well as m^*_{QO}, are considerably enhanced.

E. Mass enhancement

If the electron-electron and electron-phonon interactions are negligible, m^*_{CR} should be equal to m^*_{QO} and the masses depend only on the band structure. If there is disagreement between m^*_{CR} and m^*_{QO}, the discrepancy should arise from many-body effects due to the electron-electron and/or electron-phonon interactions. As shown in Tables II and III, in the cases of LaSb and LaBi, m^*_{CR} are reasonably consistent with m^*_{QO} and m^*_{BC}. This fact shows that both m^*_{CR} and m^*_{QO} mainly depend on the band structure if there are no $4f$ electrons. That is, the effects of both the electron-electron and electron-phonon interactions on the effective mass are small in these compounds.

However, in the case of a strongly correlated f-electron system CeSb, m^*_{CR} as well as m^*_{QO}, is considerably enhanced. This enhancement should be due to the electron-electron interaction, because there is no reason that the electron-phonon interaction strongly affects the effective mass of CeSb as compared with the mass of LaSb. It is expected that the mass enhancement due to the electron-electron interaction is large for the p bands which have the large f-electron component due to the p-f mixing. However, according to the Kohn theorem, m^*_{CR} is not affected by the intraband electron-electron interaction. This interaction conserves the whole kinetic momentum of the electrons in a band, and the conservation of the whole momentum is essential for the theorem. Therefore, our CR results, in which m^*_{CR} is also largely enhanced, indicate that the whole momentum of the electrons in a branch is not conserved. The interband electron-electron interaction and umklapp processes can break the conservation and it is possible that these interactions affect m^*_{CR}. In the case of RX, however, the pockets of the Fermi surface of the p bands are very small and are located at the Γ point. Therefore, the effect of the umklapp processes is considered to be very small. On the other hand, the effect of the interband interaction is expected to be large, because the several pockets of the p bands are located at the Γ point close to each other. Therefore, our results indicate that the interband interaction is important for the mass enhancement of m^*_{CR} in CeSb. It should be noted that the two hole pockets of the Fermi surface of LaSb are also located at the Γ point close to each other. However, the mass enhancement is negligible in LaSb. This fact shows that the p-f mixing effect is primarily important for the mass enhancement in CeSb.

In the above discussion, we stressed the importance of the interband interaction on m^*_{CR} in CeSb. However, the interband interaction also could affect m^*_{QO}. The dHvA effect measurements of CeSb under pressure show that the pressure dependence of m^*_{QO} is difficult to explain in a straightforward manner by the p-f mixing model.[25] That is, the result of the pressure dependence of m^*_{QO} could not be explained by considering the change of the f-electron content under the pressure. In this case, the interband interaction might play an important role in the mass enhancement of m^*_{QO}. However, there has been no theory to quantitatively explain the enhancement of m^*_{CR} and m^*_{QO} in real systems yet.

V. SUMMARY

We have presented detailed CR and DSCR measurements for RX. The measurements have been performed in the temperature range from 1.4 K to 40 K and in the frequency range from 50 to 190 GHz. We have observed CR signals in LaSb, LaBi, CeSb, PrSb, and GdSb. In this study, we have confirmed that the observed signals are CR, with sufficient evidence. The signals show the expected temperature, frequency, and angular dependence for CR. The estimated m^*_{CR} are reasonably consistent with m^*_{QO} and m^*_{BC}, and the values systematically change with changing R and X. We have also observed AKCR on LaSb, which also confirms our results.

This successful observation of the CR signals in RX is owing to the two experimental improvements: namely, the development of the high-frequency and high-sensitivity CR measuring system with the vector network analyzer and the remarkable improvement of the sample quality. In particular, the typical residual resistivity of our samples was about 0.1 $\mu\Omega$ cm while the typical carrier concentration in RX is two orders of magnitude smaller than those in normal metals.

The determined m^*_{CR} of LaSb, LaBi, and GdSb are in the range of $(0.17-0.65)m_0$. These values are reasonably consistent with the values of m^*_{QO} and m^*_{BC}. This fact shows that both m^*_{CR} and m^*_{QO} mainly depend on the band structure if the interaction between conduction electrons and f electrons is negligible. On the other hand, in the case of a strongly correlated f-electron system CeSb, m^*_{CR} is in the range of $(0.26-1.5)m_0$. These values are much larger than those of m^*_{BC}. This fact shows that m^*_{CR}, as well as m^*_{QO}, is considerably enhanced in CeSb. Our results indicate that the interband interaction is important for the mass enhancement of m^*_{CR} in CeSb.

ACKNOWLEDGMENTS

We are very much indebted to Professor P. C. Canfield, Dr. C. Cunningham, Dr. M. Shirakawa, Professor H. Aoki, Dr. T. Sakon, Professor H. Nojiri, and Professor K. Watanabe for valuable experimental support and discussion. This measurement was carried out at High Field Laboratory for Superconducting Materials, Institute for Materials Research, Tohoku University.

*Corresponding author. Present address: Department of Physics, Faculty of Science, Kobe University, Kobe 657-8501, Japan. Electronic address: myoshida@phys.sci.kobe-u.ac.jp

[1] J. Singleton, F. L. Pratt, M. Doporto, T. J. B. M. J. M. Kurmoo, J. A. A. J. Perenboom, W. Hayes, and P. Day, Phys. Rev. Lett. **68**, 2500 (1992).

[2] S. Hill, J. S. Brooks, Z. Q. Mao, and Y. Maeno, Phys. Rev. Lett. **84**, 3374 (2000).

[3] J. M. Schrama *et al.*, J. Phys.: Condens. Matter **13**, 2235 (2001).

[4] A. Ardavan, J. M. Schrama, S. J. Blundell, J. Singleton, W. Hayes, M. Kurmoo, P. Day, and P. Goy, Phys. Rev. Lett. **81**, 713 (1998).

[5] A. E. Kovalev, S. Hill, and J. S. Qualls, Phys. Rev. B **66**, 134513 (2002).

[6] A. E. Kovalev, S. Hill, K. Kawano, M. Tamura, T. Naito, and H. Kobayashi, Phys. Rev. Lett. **91**, 216402 (2003).

[7] E. Rzepniewski, R. S. Edwards, J. Singleton, A. Ardavan, and Y. Maeno, J. Phys.: Condens. Matter **14**, 3759 (2002).

[8] H. Matsui, A. Ochiai, H. Harima, H. Aoki, T. Suzuki, T. Yasuda, and N. Toyota, J. Phys. Soc. Jpn. **66**, 3729 (1997).

[9] Y. Oshima, H. Ohta, K. Koyama, M. Motokawa, H. M. Yamamoto, R. Kato, M. Tamura, Y. Nishio, and K. Kajita, J. Phys.

Soc. Jpn. **72**, 143 (2003).
[10] Y. Oshima, H. Ohta, K. Koyama, M. Motokawa, H. M. Yamamoto, and R. Kato, J. Phys. Soc. Jpn. **71**, 1031 (2002).
[11] Y. Oshima, M. Kimata, K. Kishigi, H. Ohta, K. Koyama, M. Motokawa, H. Nishikawa, K. Kikuchi, and I. Ikemoto, Phys. Rev. B **68**, 054526 (2003).
[12] W. Kohn, Phys. Rev. **123**, 1242 (1961).
[13] K. Kanki and K. Yamada, J. Phys. Soc. Jpn. **66**, 1103 (1997).
[14] F. Hulliger, in *Handbook on the Physics and Chemistry of Rare Earths*, edited by K. A. Gschneidner, Jr. and L. Eyring (North-Holland, Amsterdam, 1979), Vol. 4, p. 191.
[15] O. Vogt, and K. Mattenberger, in *Handbook on the Physics and Chemistry of Rare Earths*, edited by K. A. Gschneidner, Jr., L. Eyring, G. H. Lander, and G. R. Choppin (North-Holland, Amsterdam, 1993), Vol. 17, p. 301.
[16] T. Suzuki, Physica B **186–188**, 347 (1993).
[17] T. Suzuki, *Physical Properties of Actinide and Rare Earth Compounds* (Publication Office, Japanese Journal of Applied Physics, Tokyo, 1993), JJAP Series 8, p. 1131.
[18] H. Kitazawa, T. Suzuki, M. Sera, I. Oguro, A. Yanase, A. Hasegawa, and T. Kasuya, J. Magn. Magn. Mater. **31–34**, 421 (1983).
[19] R. Settai, T. Goto, S. Sakatsume, Y. S. Kwon, T. Suzuki, and T. Kasuya, Physica B **186–188**, 176 (1993).
[20] A. Hasegawa, J. Phys. Soc. Jpn. **54**, 677 (1985).
[21] K. Morita, Ph.D. thesis, Tohoku University, 1996.
[22] H. Aoki, G. W. Crabtree, W. Joss, and F. Hulliger, J. Magn. Magn. Mater. **52**, 389 (1985).
[23] H. Aoki, G. W. Crabtree, W. Joss, and F. Hulliger, J. Magn. Magn. Mater. **97**, 169 (1991).
[24] R. Settai, T. Goto, S. Sakatsume, Y. S. Kwon, T. Suzuki, Y. Kaneta, and O. Sakai, J. Phys. Soc. Jpn. **63**, 3026 (1994).
[25] M. Takashita, H. Aoki, T. Matsumoto, C. J. Haworth, T. Terashima, A. Uesawa, and T. Suzuki, Phys. Rev. Lett. **78**, 1948 (1997).
[26] M. Takashita, H. Aoki, C. J. Haworth, T. Matsumoto, T. Terashima, S. Uji, C. Terakura, T. Miura, A. Uesawa, and T. Suzuki, J. Phys. Soc. Jpn. **67**, 3859 (1998).
[27] T. Kasuya, O. Sakai, J. Tanaka, H. Kitazawa, and T. Suzuki, J. Magn. Magn. Mater. **63-64**, 9 (1987).
[28] O. Sakai, M. Takegahara, H. Harima, K. Otaki, and T. Kasuya, J. Magn. Magn. Mater. **52**, 18 (1985).
[29] Y. Kaneta, S. Iwata, T. Kasuya, and O. Sakai, J. Phys. Soc. Jpn. **69**, 2559 (2000).
[30] R. Settai, Ph.D. thesis, Tohoku University, 1992.
[31] Y. Nakanishi, T. Sakon, F. Takahashi, M. Motokawa, A. Uesawa, M. Kubota, and T. Suzuki, Phys. Rev. B **64**, 224402 (2001).
[32] Y. Nakanishi, F. Takahashi, T. Sakon, M. Yoshida, D. X. Li, T. Suzuki, and M. Motokawa, Physica B **281–282**, 750 (2000).
[33] A. Kido, S. Nimori, G. Kido, Y. Nakagawa, Y. Haga, and T. Suzuki, Physica B **186–188**, 185 (1993).
[34] K. Koyama, M. Yoshida, T. Tomimatsu, T. Sakon, D. X. Li, M. Shirakawa, A. Ochiai, and M. Motokawa, J. Phys. Chem. Solids **63**, 1227 (2002).
[35] H. Takahashi and T. Kasuya, J. Phys. C **18**, 2697 (1985).
[36] R. Settai, H. Aoki, M. Takashita, T. Terashima, Y. Haga, T. Suzuki, Y. Onuki, and T. Goto, Physica B **216**, 310 (1996).
[37] D. X. Li, Y. Haga, H. Shida, T. Suzuki, T. Koide, and G. Kido, Phys. Rev. B **53**, 8473 (1996).
[38] T. R. McGuire, R. J. Gambino, S. J. Pickart, and H. A. Alperin, J. Appl. Phys. **40**, 1009 (1969).
[39] K. Koyama, M. Yoshida, H. Nojiri, T. Sakon, D. X. Li, T. Suzuki, and M. Motokawa, J. Phys. Soc. Jpn. **69**, 1521 (2000).
[40] K. Koyama, M. Yoshida, D. X. Li, and M. Motokawa, J. Phys. Soc. Jpn. **70**, 2774 (2001).
[41] K. R. Lea, M. J. M. Leask, and W. P. Wolf, J. Phys. Chem. Solids **23**, 1381 (1962).
[42] J. Rossat-Mignod, J. M. Eeeantin, P. Burlet, T. Chattopadhyay, L. P. Regnault, H. Bartholin, C. Vettier, O. Vogt, D. Ravot, and J. C. Achart, J. Magn. Magn. Mater. **52**, 111 (1985).
[43] P. Burlet, J. Rossat-Mignod, H. Bartholin, and O. Vogt, J. Phys. (Paris) **40**, 47 (1979).
[44] M. Yoshida, K. Koyama, T. Sakon, A. Ochiai, and M. Motokawa, J. Phys. Soc. Jpn. **69**, 3629 (2000).
[45] M. Yoshida, K. Koyama, T. Tomimatsu, M. Shirakawa, A. Ochiai, and M. Motokawa, J. Phys. Soc. Jpn. **70**, 2078 (2001).
[46] M. Yoshida, K. Koyama, T. Tomimatsu, M. Shirakawa, A. Ochiai, and M. Motokawa, J. Phys. Soc. Jpn. **71**, 1752 (2002).
[47] M. Yoshida, K. Koyama, M. Shirakawa, A. Ochiai, K. Watanabe, and M. Motokawa, J. Phys. Soc. Jpn. **71**, 2847 (2002).
[48] M. Yoshida, K. Koyama, P. C. Canfield, C. Cunningham, S. Nimori, K. Watanabe, and M. Motokawa, J. Phys. Soc. Jpn. **72**, 705 (2003).
[49] M. Yoshida, K. Koyama, M. Shirakawa, A. Ochiai, K. Watanabe, and M. Motokawa, J. Phys. Soc. Jpn. **72**, 1763 (2003).
[50] M. Yoshida, K. Koyama, M. Shirakawa, A. Ochiai, K. Watanabe, and M. Motokawa, Phys. Rev. B **66**, 233107 (2002).
[51] M. Y. Azbel' and E. A. Kaner, J. Phys. Chem. Solids **6**, 113 (1958).
[52] E. A. Kaner and V. G. Skobov, Adv. Phys. **17**, 605 (1968).
[53] J. Kirsch, Phys. Rev. **133**, A1390 (1964).
[54] T. Sakon, K. Koyama, and M. Motokawa, Rev. Sci. Instrum. **73**, 1242 (2002).
[55] M. Mola, S. Hill, P. Goy, and M. Gross, Rev. Sci. Instrum. **71**, 186 (2000).
[56] O. Klein, S. Donovan, and G. Grüner, Int. J. Infrared Millim. Waves **14**, 2423 (1993).
[57] M. Yoshida, Ph.D. thesis, Tohoku University, 2002.